ELSEVIER

Chemical Geology 244 (2007) 584–604

CHEMICAL GEOLOGY
INCLUDING
ISOTOPE GEOSCIENCE

www.elsevier.com/locate/chemgeo

Trace and rare earth element geochemistry of phosphate nodules from the lower Cambrian black shale sequence in the Mufu Mountain of Nanjing, Jiangsu province, China

Shao-Yong Jiang [a,*], Hai-Xiang Zhao [a], Yong-Quan Chen [b], Tao Yang [a], Jing-Hong Yang [a], Hong-Fei Ling [a]

[a] *State Key Laboatory for Mineral Deposits Research and Center for Marine Geochemistry Research, Department of Earth Sciences, Nanjing University, Nanjing 210093, China*

[b] *Tarim Oilfield Company Exploration & Development Research Institute, Ku'erle 841000, Xinjiang Province, China*

Received 26 June 2007; accepted 7 July 2007

Editor: D. Rickard

Abstract

Phosphate nodules are abundant in the lowermost section of the Lower Cambrian black shale sequence along a NE-trend belt in the Yangtze Platform, south China. In this study, we examined the Neoproterozoic-Cambrian Mufu Mountain section near Nanjing of Jiangsu province, and conducted a detailed trace and rare earth element (REE) study on the phosphate nodules. We employed a step-leaching acid dissolution protocol of 1 M HAc and 1 M HCl, respectively, to separate carbonate from phosphate mineral contributions in the nodules. Both the HAc-leached and HCl-leached fractions of the phosphate nodules show similar symmetrical variations in trace and REE concentrations and ratios. The total REEs and a number of redox-sensitive trace metals such as V, Cr, Mo, Ni abundances show a systematic increase from the core to rim, whereas the U and Mn abundances decrease from the core to rim in most of the nodules. Similar trends are also observed for the Rb/Sr, U/Th, Co/Ni, and V/Ni ratios, but these trends in the HAc-leached fractions are less pronounced than the HCl-leached fractions. All of the HCl-leached fractions for the nodule cores show seawater-like shale-normalized REE patterns, but the rims of the nodules display slightly MREE-enriched and HREE-depleted patterns. We suggest that the phosphate nodules may have formed in a basinal setting beneath a stratified water column during Early Cambrian, and the compositional variations of REEs and redox-sensitive trace elements from the core to rim may record a changing redox condition and fluid mixing during different stages of nodule growth. The cores of the nodules preserve more pronounced negative Ce anomalies and progressively HREE-enriched patterns, which may retain primary Early Cambrian seawater chemistry, whereas the nodule rims record chemistry consistent with changed redox conditions and/or influences from pore fluids such as generated from degradation of organic matter.

Keywords: Rare earth elements; Redox-sensitive trace elements; Phosphate nodule; Black shale, Lower Cambrian, South China

1. Introduction

Phosphate nodules occur in marine sediments throughout geological history (Ilyin, 1998; Stalder and Rozendaal, 2004) and in present-day phosphate

* Corresponding author.
E-mail address: shyjiang@nju.edu.cn (S.-Y. Jiang).

0009-2541/$ - see front matter © 2007 Published by Elsevier B.V.
doi:10.1016/j.chemgeo.2007.07.010

sediments (Rasmussen et al., 1998). The phosphate sediments occur in organic-rich, diatomaceous sediments, for example, in South Africa, Peru-Chile and Baja California (Veeh et al., 1973; Birch, 1979; Schuffert et al., 1994), all of the areas have a very high bioproductivity in the world (Walsh, 1981). However, phosphates are also found in low-productivity oceans, in which case bacteria and organic materials probably played an important role in the assimilation of phosphorus (O'Brein et al., 1981).

It is well known that phosphate nodules can incorporate abundant rare earth elements (REE) during their growth in marine sediments during very early diagenesis (Kidder et al., 2003). The REE concentrations, shale-normalized REE patterns, and Ce and Eu anomalies in the phosphate nodules and phosphorites are useful indicators of post-marine depositional environments. For example, the middle REE-enriched (MREE, defined as Sm–Ho) shale-normalized REE patterns (the so called "hat" pattern) commonly exist in many phosphate sediments, such as biogenic apatites (Wright et al., 1987; Grandjean-Lecuyer et al., 1993), the "old phosphorites" (Ilyin, 1998), phosphate nodules (Tlig et al., 1987), and apatite stromatolites (Bertrand-Sarfati et al., 1997). It is suggested that this type of REE pattern is caused by diagenetic alteration (German and Elderfield, 1990; Shields and Stille, 2001). As a result, these samples rarely retain primary seawater REE distribution patterns with a characteristically progressive enrichment in the heavier REEs and pronounced negative Ce anomaly. Ilyin (1998) found that almost all phosphorites older than Mesozoic yield socalled "old phosphorite" REE patterns, which contain pronounced negative Ce anomaly and depletion in heavy REE (HREE, from Ho to Lu). In contrast, the seawater-like REE patterns with a negative Ce anomaly and progressively heavier REE enrichment are only common in some post-Jurassic phosphates (Shields and Stille, 2001). In this study, we report seawater-like REE patterns for the phosphate nodules from the Lower Cambrian black shales in the Yangtze Platform of South China, and together with a number of redox-sensitive trace elements, we discuss their significance on contemporary seawater chemistry, diagenetic processes, and palaeo-ocean environments.

2. Geological setting and studied section

Phosphate nodules widely exist in the Lower Cambrian black shales, and they are particular abundant in the lowermost section just below a conspicuous Ni–Mo sulfide ore layer in the Yangtze platform, south China

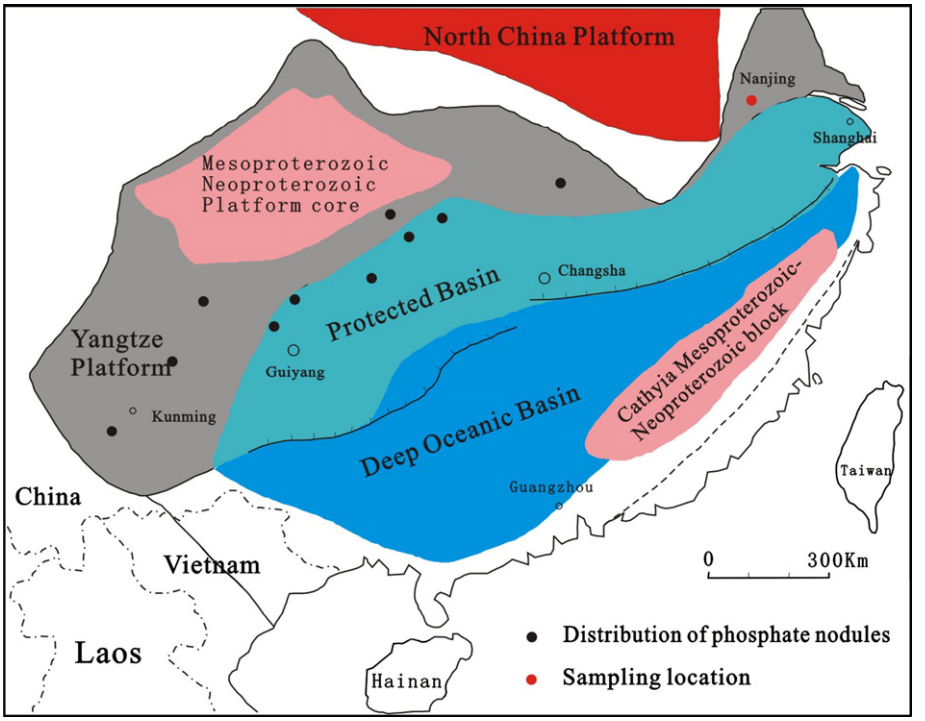

Fig. 1. Sketch map of Yangtze platform during Precambrian–Cambrian interval, and the distribution of phosphate nodules in Lower Cambrian strata.

(Chen et al., 2003; Yang et al., 2004; Jiang et al., 2006, in press). It is worth noting that all phosphate nodules exist above the hiatus surfaces (Zhu et al., 2003) in the Lower Cambrian strata in South China, consistent with what is reported by Kennedy and Garrison (1975) and Marshall-Neil and Ruffell (2004). Fig. 1 shows the palaeogeographic conditions of Yangtze platform and the distributions of phosphate nodules during early Cambrian. From the diagram we can distinguish three distinct facies regions (Steiner et al., 2001; Zhu et al., 2003): carbonate platform, protected basin, and deep-ocean basin (Fig. 1).

In the Mufu Mountain near Nanjing of Jiangsu province, a typical Neoproterozoic to Cambrian section is exposed in the open pits of a dolomite mine. The Mufu Mountain section consists of three formations, from bottom to top, the Neoproterozoic Dengying Formation of dolostone; the Early Cambrian Mufu Mountain Formation composed of black shales with phosphate nodules and interbedded siliceous rocks; and the Early-Middle Cambrian Paotaishan Formation composed of chert nodule-bearing dolostone (Fig. 2).

3. Samples and analytical methods

Six representative phosphate nodules were collected during this study from the lowermost part of the Early Cambrian black shale sequence in the Mufu Mountain section (Fig. 3A,B). The phosphate nodules were sliced into two halves (Fig. 3C). In each nodule sample, we used an electric drill to collect sample powders from core (C) to rim (L and R), and five samples (L2, L1, C,

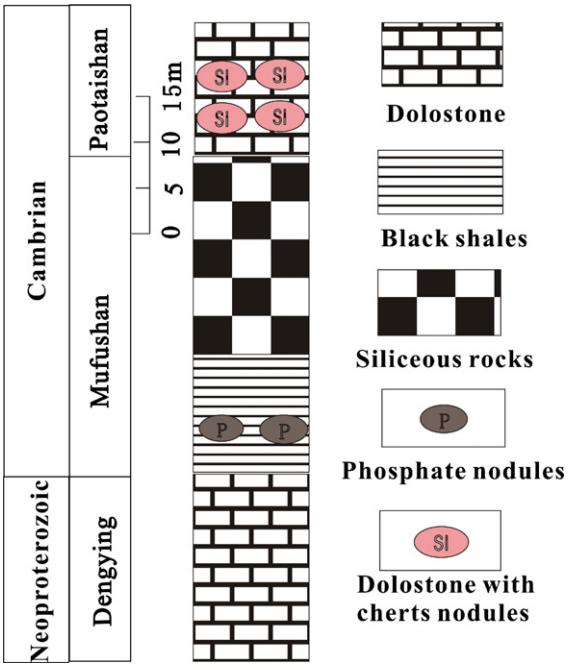

Fig. 2. Sketch stratigraphic column showing the Neoproterozoic–Cambrian sequence in the Mufu Mountain section near Nanjing of Jiangsu province.

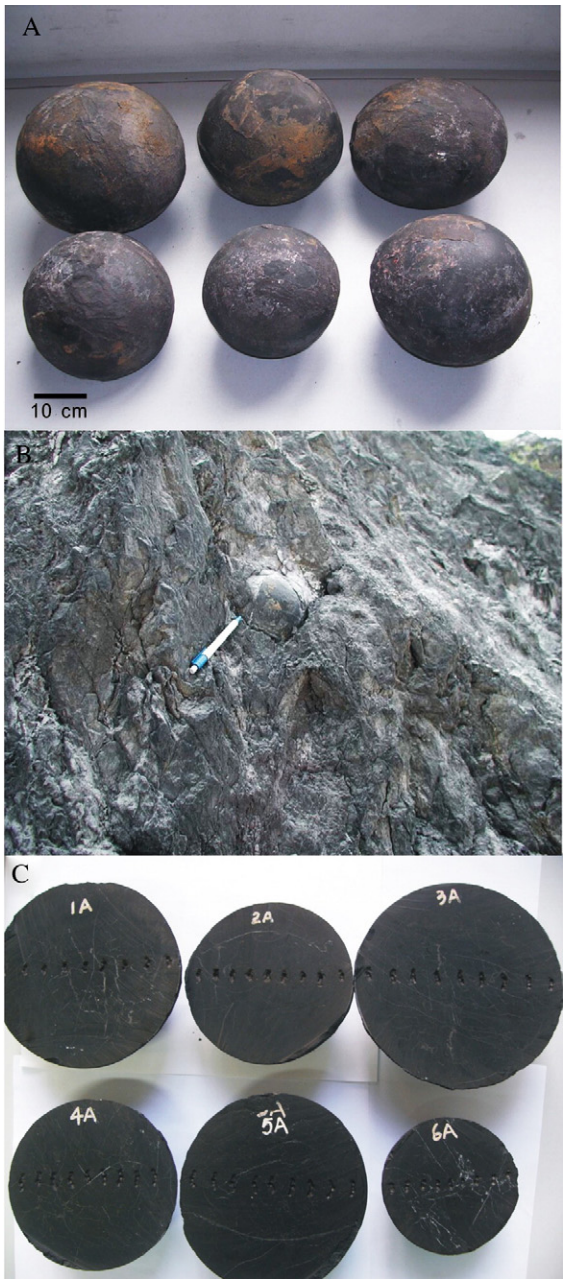

Fig. 3. Photos for phosphate nodules from the lowermost part of the Early Cambrian black shale sequence in the Mufu Mountain section near Nanjing of Jiangsu province. A) six selected whole nodules, B) outcrop of nodule-bearing black shale, C) six selected half-cutted nodule sections.

Table 1
Electron microprobe analyses for major elements in phosphate nodules

Sample spot	Mineral phase	CaO	P_2O_5	SiO_2	Al_2O_3	MgO	FeO	MnO	SrO	BaO	F	SO_3	Total
L4	Phosphate	54.60	44.02	0.034	0.002	0.085	0.048	0.000	0.000	0.000	0.077	0.198	99.03
L3	Phosphate	53.59	41.64	0.035	0.000	0.005	0.045	0.013	0.092	0.000	0.034	0.256	95.70
L2	Phosphate	49.84	39.89	1.77	0.146	0.004	0.172	0.000	0.098	0.112	0.019	0.332	92.37
L1	Phosphate	52.36	39.06	0.160	0.008	0.000	0.000	0.036	0.000	0.059	0.024	0.250	91.94
R1	Phosphate	50.43	38.21	1.009	0.005	0.005	0.009	0.000	0.069	0.105	0.012	0.312	90.16
R2	Phosphate	52.27	39.99	0.715	0.005	0.000	0.019	0.010	0.097	0.098	0.006	0.277	93.48
R3	Phosphate	50.67	40.26	0.402	0.000	0.000	0.000	0.000	0.058	0.099	0.000	0.260	91.74
R4	Phosphate	54.53	42.65	0.022	0.000	0.000	0.000	0.010	0.000	0.020	0.019	0.222	97.46

R1, R2) were collected for each nodule. Because the nodules contain crosscutting veinlets within them, we have tried to avoid these vein materials and choose only those areas where macroscopically observable veinlets were absent to extract the phosphate nodule samples. Petrographic observations show that the nodules are mainly composed of microcrystalline apatite (francolite) and organic matters, without pellets and fecal fabrics.

About 100 mg of each sample were weighted in Teflon beakers and leached by 1 M HAc under an ultrasonic bath for several hours to dissolve the carbonate fractions in the nodule samples. The residues were then dissolved in 1 M HCl on a hotplate at about 120 °C overnight to dissolve the phosphate fractions. After dissolution, the sample solutions were centrifuged, and the supernatants were transferred to clean Teflon beakers, then the solutions were evaporated to near dryness, 1 ml concentrated HNO_3 was then added and dried twice to get rid of the HAc or HCl in the samples. Finally the samples were dissolved in 5% HNO_3 solution spiked with an internal standard Rh (10 ppb) for analysis. All the samples were analyzed by high resolution inductively coupled plasma mass spectroscopy (HR-ICP-MS) technique at State Key Laboratory for Mineral Deposits Research of Nanjing University. In order to keep the Ba interference into minimum, we adopted a membrane desolvating sample introduction system (Aridus, CETAC, USA) during ICP-MS measurement. The analytical precision is estimated to be <10% according to duplicate analysis of samples and standards.

Major element concentrations of the nodules were analyzed using a JEOL JXA-8800 electron microprobe at State Key Laboratory for Mineral Deposits Research at Nanjing University, China. Element determinations (Ca, P, Si, Al, Fe_{Total}, Mg, Mn, Ba, Sr, F and S) were carried out using a beam size of 3 μm, an accelerating potential voltage of 15KV, and a probe current of 15 nA. Standards used were natural minerals and synthetic compounds, including hornblende (Si, Na, Mg, Al, Ca, Ti), apatite (F), fayalite (Fe, Mn), and K-feldspars (K) in the analytical procedure. Matrix effects were corrected using the ZAF software provided by JEOL.

4. Results

4.1. Major element compositions

Generally, the nodules are almost completely composed of phosphate minerals with contents of CaO ranging from 49.8 to 54.6 wt.% and those of P_2O_5 from 38.2 to 44.0 wt.%. Other oxide concentrations are general less than 0.1 wt.%, however, the sulfur contents vary from 0.20 to 0.33 wt.% SO_3 (Table 1). The contents of major element P_2O_5 and CaO show concave patterns in the nodule traverse, increasing form the core to rim with values range of 42.6% to 44.0% (P_2O_5) and 54.5% to 54.6% (CaO) in the rims (R4 and L4 in Table 1), and 38.2% to 41.6% (P_2O_5) and about 50% (CaO) in the cores (C).

4.2. Rare earth element (REE) compositions

REE results of both the HAc-leached and HCl-leached fractions of the six phosphate nodules are listed in Table 2 and 3, respectively.

The total REE concentrations of the nodules show a large variation, with the HCl-leached fractions from 6.4 to 701.5 ppm and the HAc-leached fractions from 9 to 126 ppb (Table 2). The low absolute REE abundances in the HAc-leached fraction are due to the very low concentration of carbonate in the nodules and the concentration values are calculated based on the bulk sample weight before leaching. Both the HCl-leached and HAc-leached fractions of the nodules display general symmetrical variations in total REE concentration with values increasing from the cores and inner layers to the outer rims (Fig. 4).

In the six nodule traverses, the HCl-leached fractions of the cores and inner layers (C, L1 and R1) show a pronounced negative Ce anomaly and a characteristically

Table 2
Analytical results of REE concentrations for the HAc-leached fractions of the phosphate nodules

ppb	1C	1L1	1L2	1R1	1R2	2C	2L1	2L2	2R1	2R2	3C	3L1	3L2	3R1	3R2
La	11.4	11.2	11.0	15.3	19.0	3.1	2.9	4.0	3.2	5.6	3.2	2.5	4.8	2.4	3.9
Ce	6.0	10.6	16.6	16.7	34.3	5.5	8.2	4.8	4.0	10.0	0.6	0.9	8.5	3.7	4.0
Pr	2.2	2.3	3.7	3.5	8.1	0.8	0.9	1.3	1.1	2.2	2.2	0.9	2.8	0.7	2.3
Nd	9.0	5.6	10.2	7.4	24.6	1.1	1.3	1.7	1.1	4.2	1.9	1.6	6.2	1.4	3.3
Sm	1.8	1.6	1.9	1.4	5.3	0.1	0.2	0.3	0.3	1.1	0.3	0.3	2.0	0.2	0.9
Eu	4.2	4.0	4.8	4.9	4.4	3.5	2.3	3.4	3.4	2.9	1.9	1.5	2.2	1.4	1.6
Gd	3.4	2.9	4.9	4.1	8.8	0.6	0.6	1.0	0.6	1.6	1.4	1.1	3.2	0.8	1.7
Tb	0.4	0.4	0.5	0.5	1.1	0.1	0.1	0.1	0.1	0.2	0.1	0.1	0.4	0.1	0.2
Dy	2.8	2.3	3.9	2.7	8.1	0.3	0.3	0.8	0.3	1.2	0.5	0.5	2.5	0.4	1.3
Ho	0.8	0.6	1.1	0.8	2.0	0.03	0.04	0.1	0.0	0.2	0.2	0.1	0.7	0.1	0.3
Er	2.3	2.0	2.8	2.9	5.7	0.1	0.1	0.6	0.1	0.8	0.3	0.4	2.1	0.2	1.0
Tm	0.4	0.3	0.3	0.5	0.6	0.01	0.02	0.05	0.03	0.1	0.04	0.05	0.3	0.05	0.1
Yb	2.5	2.2	1.8	2.9	3.5	0.1	0.1	0.5	0.2	0.5	0.2	0.3	1.7	0.4	0.8
Lu	0.4	0.4	0.4	0.5	0.6	0.00	0.00	0.00	0.00	0.00	0.00	0.00	0.00	0.00	0.00
TREE	47.6	46.3	63.8	64.1	126	15.3	17.0	18.5	14.4	30.6	12.9	10.1	37.4	11.9	21.4
Y	51.8	42.1	43.2	55.1	86.2	3.9	3.4	13.1	5.5	15.0	7.5	7.0	31.9	5.9	17.0
Y/Ho	65.1	71.3	40.8	65.0	43.1	143.0	85.2	97.6	113.6	60.3	46.6	72.9	43.1	56.8	50.6
Eu/Eu*	7.70	8.65	7.24	9.21	2.95	53.34	32.50	26.51	38.29	10.19	12.91	11.59	4.09	14.34	5.79
Ce/Ce*	0.25	0.47	0.71	0.56	0.77	0.96	1.54	0.62	0.66	0.84	0.10	0.18	0.67	0.77	0.45

ppb	4C	4L1	4L2	4R1	4R2	5C	5L1	5L2	5R1	5R2	6C	6L1	6L2	6R1	6R2
La	3.6	2.5	3.7	2.7	4.3	8.8	8.9	13.8	6.1	19.1	7.9	8.0	6.8	3.8	10.0
Ce	2.8	0.7	4.8	0.2	5.2	10.9	8.5	17.6	3.8	33.0	8.0	5.9	4.2	1.7	11.8
Pr	2.3	0.9	2.5	1.0	5.0	1.8	1.5	3.9	0.8	7.5	1.9	1.2	1.5	0.5	2.6
Nd	2.9	1.1	4.5	1.1	6.3	3.3	5.1	17.0	3.1	36.4	8.6	3.4	6.7	1.5	11.8
Sm	0.7	0.2	1.6	0.4	2.3	0.6	1.2	4.2	0.5	9.3	3.1	0.5	1.5	0.3	3.6
Eu	2.0	1.5	1.7	1.5	2.2	1.3	1.4	2.3	0.8	3.4	1.9	1.2	1.4	1.0	1.9
Gd	1.5	0.8	3.1	0.7	4.4	0.9	2.4	7.8	1.6	13.1	5.3	1.6	3.7	0.9	7.9
Tb	0.2	0.1	0.3	0.1	0.5	0.2	0.3	1.3	0.2	1.8	1.0	0.2	0.6	0.1	1.1
Dy	1.0	0.4	2.9	0.3	4.0	0.9	2.0	6.9	1.1	11.9	5.4	1.0	3.1	0.5	7.3
Ho	0.2	0.1	0.7	0.1	0.9	0.2	0.5	1.8	0.4	2.8	1.4	0.3	0.9	0.1	2.1
Er	0.5	0.4	1.8	0.1	2.4	0.8	1.6	5.3	1.1	7.1	4.3	1.0	2.3	0.3	5.9
Tm	0.1	0.03	0.2	0.02	0.3	0.1	0.3	0.6	0.2	0.8	0.6	0.1	0.2	0.1	0.7
Yb	0.4	0.3	1.1	0.2	1.7	1.0	1.8	3.8	1.0	3.7	3.3	1.0	1.9	0.4	3.5
Lu	0.00	0.00	0.00	0.00	0.00	0.2	0.3	0.8	0.2	0.8	0.7	0.2	0.4	0.1	0.8
TREE	18.2	9.0	28.8	8.4	39.5	30.9	35.6	87.3	20.8	150.7	53.4	25.7	35.1	11.3	71.0
Y	11.6	7.3	28.8	5.1	42.2	17.9	26.4	67.0	19.1	80.8	55.9	18.8	39.7	7.0	88.8
Y/Ho	56.8	55.2	41.4	66.3	45.8	73.2	56.4	36.9	43.5	29.1	40.5	55.0	45.0	59.4	42.1
Eu/Eu*	9.09	17.1	3.46	14.0	3.19	8.56	3.87	1.86	4.43	1.40	2.19	6.71	2.70	9.49	1.60
Ce/Ce*	0.36	0.14	0.49	0.04	0.42	0.66	0.47	0.53	0.33	0.61	0.39	0.40	0.28	0.24	0.47

progressive enrichment of HREE in the shale-normalized REE distribution patterns (Fig. 5), which are quite similar to those of the seawater. Most of the outer rims of the nodules (L2 and R2) show slightly MREE-enriched and LREE-and HREE-depleted curves (the so called "hat" pattern) in the shale-normalized REE distribution patterns (Fig. 5). In contrast, the HAc-leached fractions show a rather flat shale-normalized REE distribution curves (Fig. 6) both for the core and rim, and the outer rims (L2 and R2) also have higher total REE concentrations.

In the HAc-leached fractions, there are pronounced positive Eu anomalies with Eu/Eu* from 1.4 to 53.3 (Table 2). Due to the extremely high Ba/Eu ratios in these samples, these positive Eu anomalies are likely artfacts caused by Ba interference during ICP-MS measurement, as indicated by the excellent linear correlation between Ba/Sm and Eu/Eu* (Fig. 7a). Therefore, we will not discuss the Eu anomaly in these samples. However, the lower Ba/Eu ratios and lack of Ba/Sm and Eu/Eu∗ correlation in the HCl-leached fractions (Fig. 7b) suggest that the Eu anomaly in these samples are real and can be used as genetic indicators. In Nodules 2, 3, 4, and 6, the outer rims show higher Eu/Eu* values than the cores (Fig. 8), but the Eu/Eu* values in the Nodule 5 show a decrease from the core to rim (Fig. 8). The Eu/Eu* variation in the Nodule 1

Table 3
Analytical results of REE concentrations for the HCl-leached fractions of the phosphate nodules

ppm	1C	1L1	1L2	1R1	1R2	2C	2L1	2L2	2R1	2R2	3C	3L1	3L2	3R1	3R2
La	23.7	36.7	53.4	34.7	64.5	2.09	2.80	11.1	4.48	11.3	3.94	3.56	5.27	4.06	5.68
Ce	15.5	21.9	63.2	20.8	86.9	1.78	2.14	9.34	3.10	14.3	3.55	3.55	6.24	3.70	5.81
Pr	3.77	4.13	12.68	3.23	19.1	0.30	0.34	1.77	0.47	3.14	0.70	0.80	1.95	0.74	1.38
Nd	18.5	18.9	52.1	14.1	81.6	1.07	1.23	7.32	1.66	15.3	2.96	3.70	11.3	3.39	6.41
Sm	4.52	4.62	10.1	2.52	17.1	0.18	0.21	1.54	0.26	3.37	0.58	0.85	3.49	0.71	1.92
Eu	1.45	1.46	3.04	0.89	4.72	0.05	0.08	0.79	0.09	1.43	0.20	0.27	1.32	0.22	0.91
Gd	7.84	7.70	16.17	5.32	26	0.21	0.27	3.02	0.42	5.52	1.02	1.42	6.26	1.18	3.72
Tb	1.03	1.02	2.33	0.73	3.61	0.03	0.04	0.40	0.06	0.73	0.13	0.20	0.85	0.16	0.49
Dy	7.40	7.90	18.0	6.49	25.7	0.20	0.31	3.12	0.48	5.28	0.98	1.44	6.03	1.19	3.48
Ho	1.81	2.10	4.30	1.97	5.76	0.05	0.09	0.85	0.17	1.24	0.27	0.37	1.45	0.32	0.87
Er	5.79	7.14	11.9	7.02	15.1	0.18	0.37	2.61	0.61	3.18	0.84	1.17	4.15	1.00	2.49
Tm	0.92	1.19	1.55	1.13	1.88	0.03	0.06	0.33	0.10	0.37	0.11	0.16	0.54	0.14	0.33
Yb	6.67	7.30	8.01	7.48	9.30	0.19	0.45	1.90	0.61	1.89	0.68	1.07	3.21	0.82	1.94
Lu	1.18	1.30	1.12	1.17	1.26	0.04	0.09	0.28	0.11	0.27	0.11	0.18	0.49	0.14	0.29
TREE	100.0	123.4	258.0	107.5	362.3	6.4	8.5	44.4	12.6	67.3	16.1	18.7	52.5	17.8	35.7
Y	125	152	191	139	226	3.3	8.0	51.7	12.9	56.9	14.2	18.4	60.7	15.5	39.7
Y/Ho	68.8	72.4	44.4	70.5	39.2	62.0	84.2	60.7	77.1	45.9	52.1	49.9	42.0	47.8	45.7
Eu/Eu*	1.11	1.12	1.09	1.11	1.03	1.15	1.45	1.69	1.21	1.51	1.19	1.12	1.29	1.08	1.56
Ce/Ce*	0.30	0.30	0.55	0.32	0.58	0.44	0.40	0.41	0.37	0.53	0.44	0.44	0.37	0.43	0.41

ppm	4C	4L1	4L2	4R1	4R2	5C	5L1	5L2	5R1	5R2	6C	6L1	6L2	6R1	6R2
La	4.16	3.73	6.50	3.57	6.49	23.4	19.7	42.5	47.9	101.2	10.2	10.8	17.7	5.45	20.3
Ce	4.25	3.87	7.97	2.87	8.38	9.57	11.2	44.3	30.5	148	10.1	7.33	17.95	3.67	24.2
Pr	0.94	0.84	2.71	0.52	2.56	1.32	2.23	10.24	5.51	38.2	2.30	1.35	4.11	0.68	5.91
Nd	4.79	4.81	17.2	2.20	16.6	5.09	9.38	55.0	22.9	185	13.2	5.98	23.1	2.81	30.7
Sm	1.58	1.90	7.44	0.52	7.78	0.86	1.98	13.3	3.8	45.8	4.37	1.10	5.68	0.57	8.58
Eu	0.52	0.64	3.02	0.20	3.19	0.37	0.69	4.02	1.39	11.42	1.30	0.37	2.22	0.17	2.99
Gd	2.75	3.57	13.8	0.96	14.78	1.99	3.74	23.0	8.92	58.9	8.95	2.01	11.5	0.98	17.05
Tb	0.36	0.51	1.77	0.13	1.95	0.27	0.49	3.22	1.26	7.59	1.22	0.27	1.42	0.14	2.20
Dy	2.48	3.78	11.6	1.01	12.8	2.46	3.98	22.5	10.9	50.0	9.02	2.10	9.82	1.10	15.8
Ho	0.61	0.95	2.59	0.28	2.86	0.88	1.18	5.41	3.29	10.3	2.40	0.62	2.48	0.33	3.83
Er	1.78	2.76	6.50	0.92	7.34	3.58	4.01	15.1	10.8	24.9	6.95	2.00	6.75	1.17	10.3
Tm	0.23	0.37	0.77	0.13	0.86	0.57	0.63	1.85	1.52	3.08	0.88	0.27	0.83	0.18	1.25
Yb	1.38	2.16	4.17	0.83	4.47	4.06	4.36	10.65	9.26	15.58	4.83	1.71	4.46	1.23	6.61
Lu	0.22	0.34	0.58	0.14	0.61	0.81	0.80	1.55	1.45	2.00	0.68	0.28	0.65	0.22	0.92
TREE	26.1	30.2	86.6	14.3	90.7	55.3	64.3	252.7	159.4	701.5	76.4	36.1	108.7	18.7	150.7
Y	30.6	43.2	113	15.8	126	78.5	77.4	219	178	358	97.5	40.3	120	20.5	186
Y/Ho	50.0	45.4	43.6	55.9	44.0	88.8	65.6	40.5	53.9	34.7	40.7	65.4	48.5	61.7	48.6
Eu/Eu*	1.14	1.13	1.36	1.29	1.36	1.30	1.15	1.05	1.10	1.01	0.95	1.13	1.26	1.06	1.13
Ce/Ce*	0.40	0.36	0.29	0.39	0.29	0.23	0.29	0.43	0.34	0.53	0.37	0.35	0.41	0.34	0.45

are less significant (Fig. 8). Negative Ce anomalies are observed for all of the nodules. Nodule 1 and 5 show a significant increase of Ce/Ce* values from the cores to rims, whereas the variations of Ce/Ce* are less significant in the other nodules (Fig. 8).

4.3. Selected trace element compositions

Results of the selected trace elements, in particular those redox-sensitive trace elements, for both the HAc-leached and HCl-leached fractions of the six phosphate nodules are listed in Table 4 and 5, respectively.

In the HCl-leached fractions, concentrations of Sr and Ba are extremely high from 1120 to 2792 ppm and 817 to 6144 ppm, respectively. Concentrations of Mn, V, Ti, Zn, and Cr are also high and in the ranges of several tens ppm, and concentrations of Mo, Ni, Sc, Co, Cu, Ga, Rb, Pb, U, and Th are in the ranges of sub-ppm to several ppm (Table 5). It is evident that concentrations of Mn and U decrease from the core to rim, whereas concentrations of V, Cr, Mo, and Ni increase from the core to rim (Fig. 9). A decrease trend is also observed for the U/Th, Co/Ni and V/Ni ratios, but the Rb/Sr ratios show an increase from the core to rim (Fig. 10).

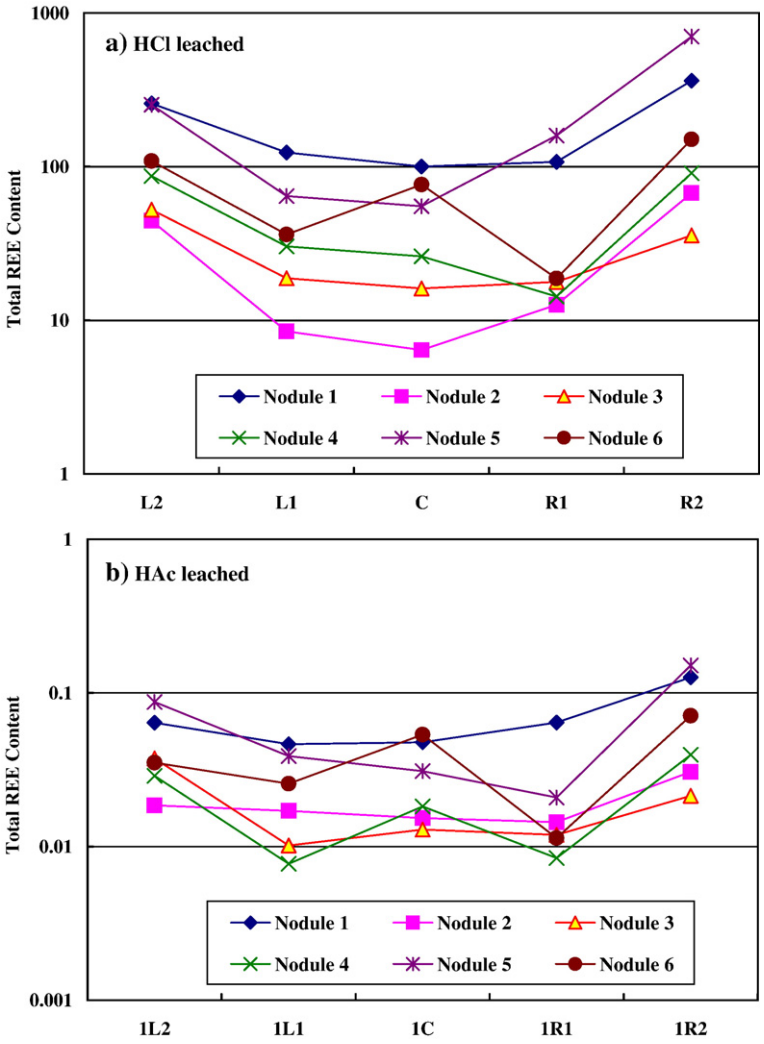

Fig. 4. Total REE concentration variation from the core to the rim for the phosphate nodules. (a) HCl-leached fractions; (b) HAc-leached fractions.

In the HAc-leached fractions, concentrations of Mn. Ni, Co, Sr, and Ba are relatively high in the ranges of several ppm to hundreds ppm. But other trace elements are all low (<3 ppm, Table 4). The trace element traverse trends from the core to rim are generally similar to the HCl-leached fractions, but are less significant and/or absent in some nodules (Table 4).

5. Discussion

5.1. Rare earth element (REE) systematics

Our data show that the total REE concentrations are higher in the outer rims than in the cores and inner portions of the phosphate nodules, which are broadly similar to the results obtained for phosphate nodules from black shales of the Pennsylvanian-age and Mississipian-age deposits in the USA (Kidder et al., 2003). It is likely that the outer rims equilibrated with the pore fluids that had a greater enrichment in REE during the process of diagenesis. The late stage pore fluids may have obtained more REE from the organic matters and host black shales, which may then have been incorporated into the outer layers of phosphate nodules during progressive nodule growth and diagenesis. In a study of the Early Cambrian phosphorites in Yunan and Sichuan provinces of south China, Shields and Stille (2001) suggested that during diagenetic mineralization, phosphorites contain progressively greater REE contents due to early REE scavenging in sediment pore waters. Elderfield and Sholkovitz (1987) reported high REE concentrations

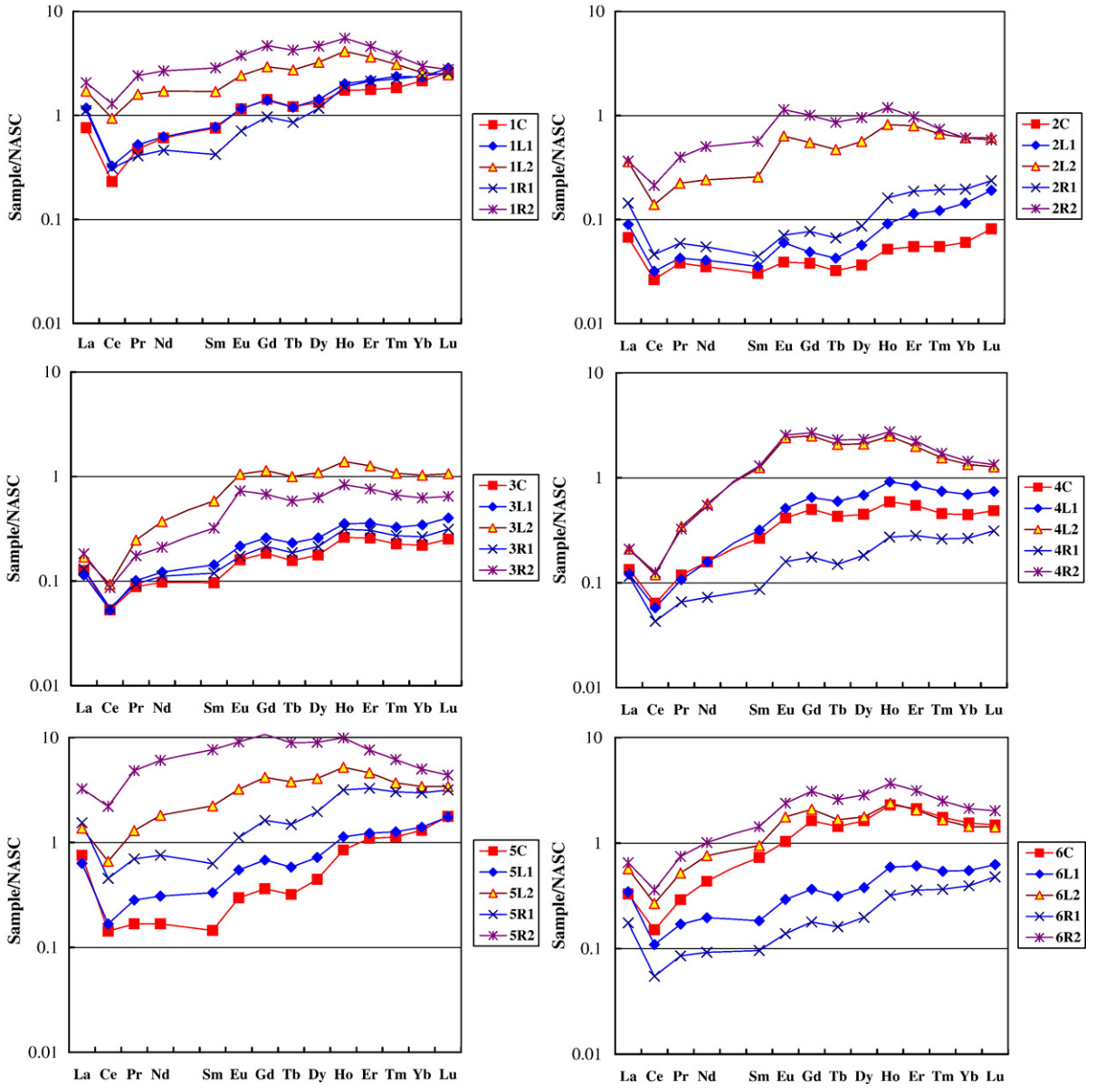

Fig. 5. Shale-normalized REE distribution patterns of studied phosphate nodule traverse for the HCl-leached fractions.

in pore waters in reducing nearshore sediments. It is suggested that the high REE concentrations in pore waters are due to REE mobility and release of REE, without fractionation, from sediments during early diagenesis (Elderfield and Sholkovitz, 1987). These authors suggested that preferential Ce enrichment (positive Ce anomalies) and preferential heavy REE enrichment (or light REE removal) in the pore waters are associated with redox cycling of Fe and Mn in the sediments (Elderfield and Sholkovitz, 1987; Sholkovitz et al., 1989).

In general, all of the HCl-leached fractions for the phosphate nodule cores show a seawater-like light REE depleted and middle and heavy REE enriched shale-normalized pattern (Fig. 5). We suggest that the phosphate nodule cores may have recorded the seawater REE characteristics that did not altered by post depositional, diagenetic exchange. In contrast, the rims of the phosphate nodules show a middle REE enriched and HREE depleted pattern (Fig. 5), which is a typical feature for those phosphorites that underwent diagenetic alteration (Wright et al., 1987; Shields and Stille, 2001). Previous

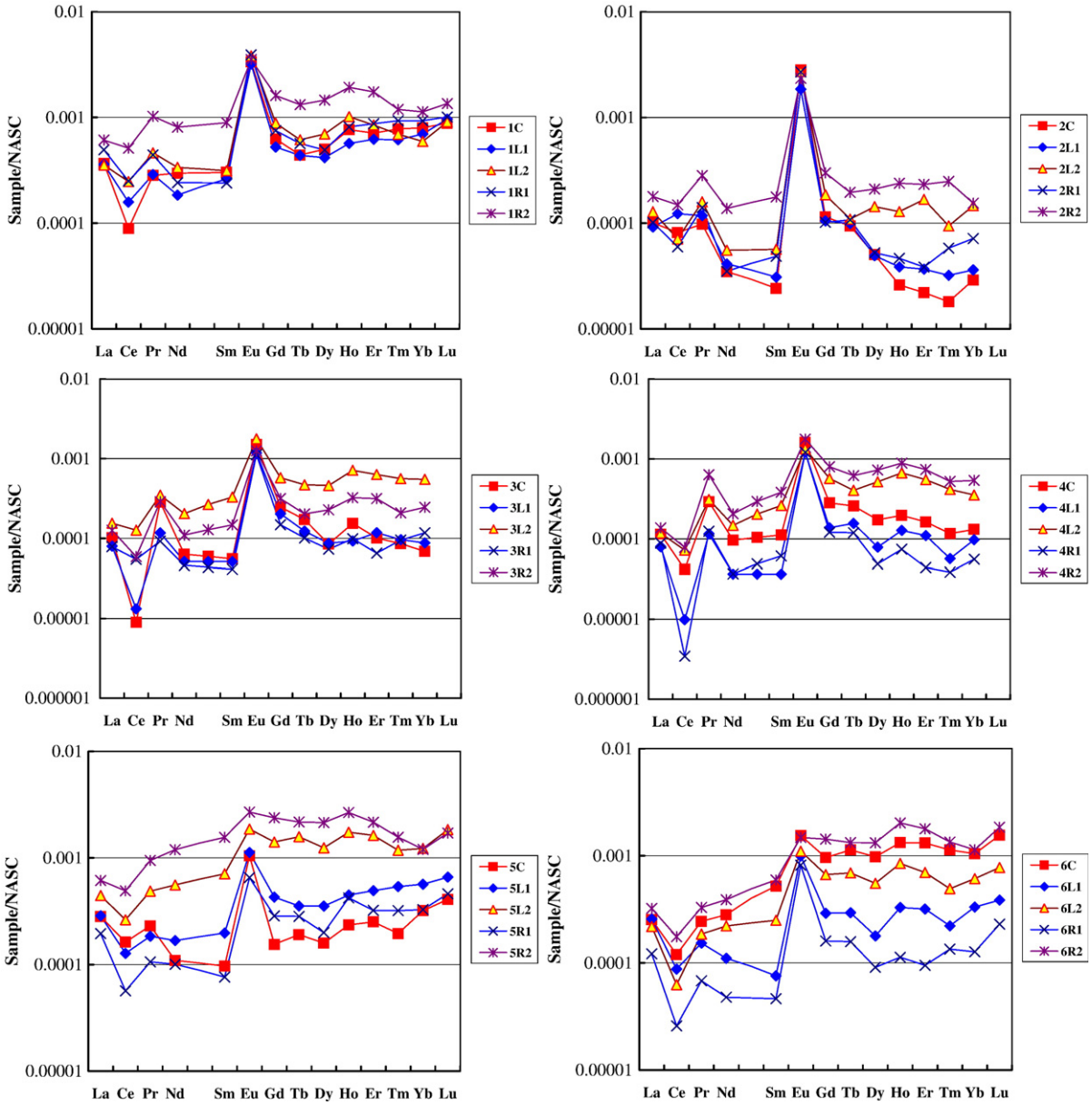

Fig. 6. Shale-normalized REE distribution patterns of studied phosphate nodule traverse for the HAc-leached fractions.

studies have reported that the seawater-like REE patterns are only common in some post-Jurassic phosphates (Shields and Stille, 2001). Almost all phosphorite older than Mesozoic yielded so-called "old phosphorite" REE patterns (Ilyin, 1998), which are similar to those REE patterns for the phosphate nodule rims in this study. Some researchers have suggested that these "old phosphorite" patterns faithfully reflect pre-Mesozoic seawater, which was depleted in HREE (McArthur and Walsh, 1984; Ilyin, 1998; Picard et al., 2002). Our data certainly did not support this view. Instead, we suggest the REEs in the Early Cambrian seawater are the same as the modern seawater, as recorded in the cores of phosphate nodules. The "old phosphorite" REE patterns reflect diagentic effects away from primary seawater signatures, as are the cases for the rims of the studied phosphate nodules. The finding of seawater-like REE patterns in the Early Cambrian phosphate cores in this study may provide us a new approach to study the pre-Mesozoic seawater chemistry.

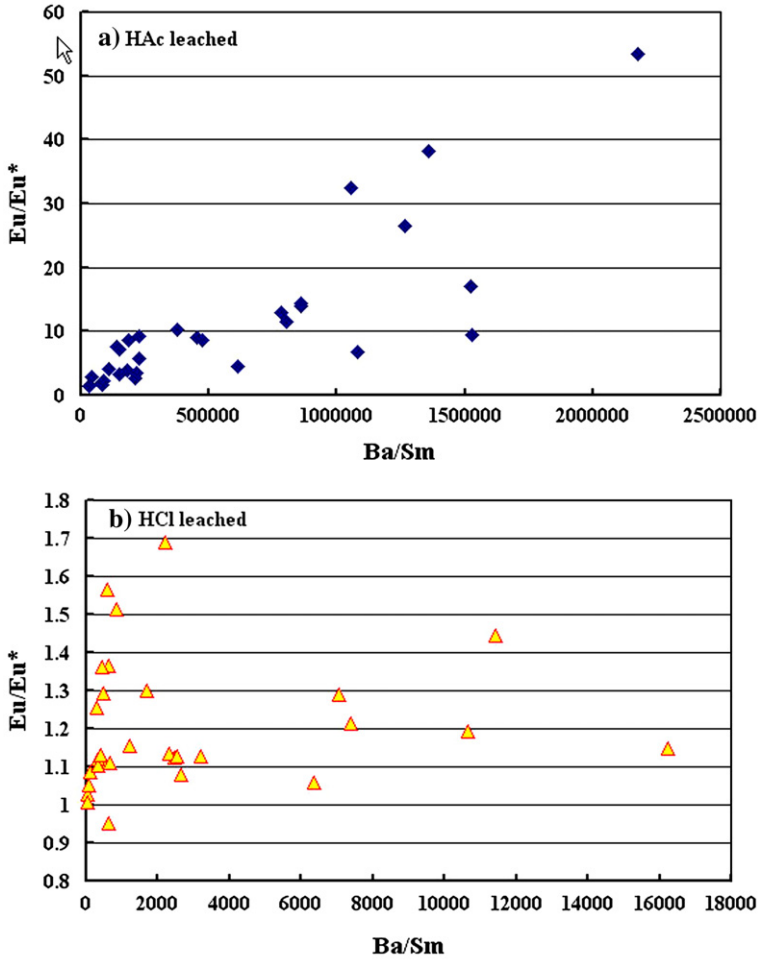

Fig. 7. Correlation between Eu/Eu* and Ba/Sm of the phosphate nodules. a) HAc-leached fractions; b) HCl-leached fractions.

It is likely that organic matters in host black shales may contribute to the MREE enrichment for the rims of the studied phosphate nodules. Kidder and Eddy-Dilek (1994) suggested that algae and/or bacteria were selectively enriched in MREE in the genesis of the Kansas and Oklahoma phosphates. Elderfield et al. (1990) found that organic-rich and/or oxy-hydroxide grain coatings in the Tamar Estuary, England are enriched in MREE. Through a laboratory experiment, Stanley and Byrne (1990) discovered that the green alga could preferentially take up the MREE.

We suggested that primary pore water and later fluid produced by diagenesis and organic matter decomposition may have been responsible for the phosphate nodule growth, and the primary pore water was similar to seawater in chemistry because the phosphate nodules initially formed at or near the interface between seawater and sediments. As reported by Elderfield and Pagett (1986), biogenic phosphates can acquire seawater-like REE patterns during early diagenesis close to water–sediment interface. Nodules formed during early diagenesis can incorporate REE from pore water and diagenetic fluids, and may distill REE from humic acid only if organism in host shales had cracked before nodules formed. Therefore, if nodules had formed before cracking of organic material, the nodules would retain seawater-like pore water REE characteristics. If nodules had formed after cracking of organic material, the nodules would show a MREE-rich pattern of diagenetic origin.

5.2. Eu anomaly

A Eu anomaly is a common geochemical phenomenon due to different valences of Eu compared to the strictly trivalent valence typical of other REEs (De Baar

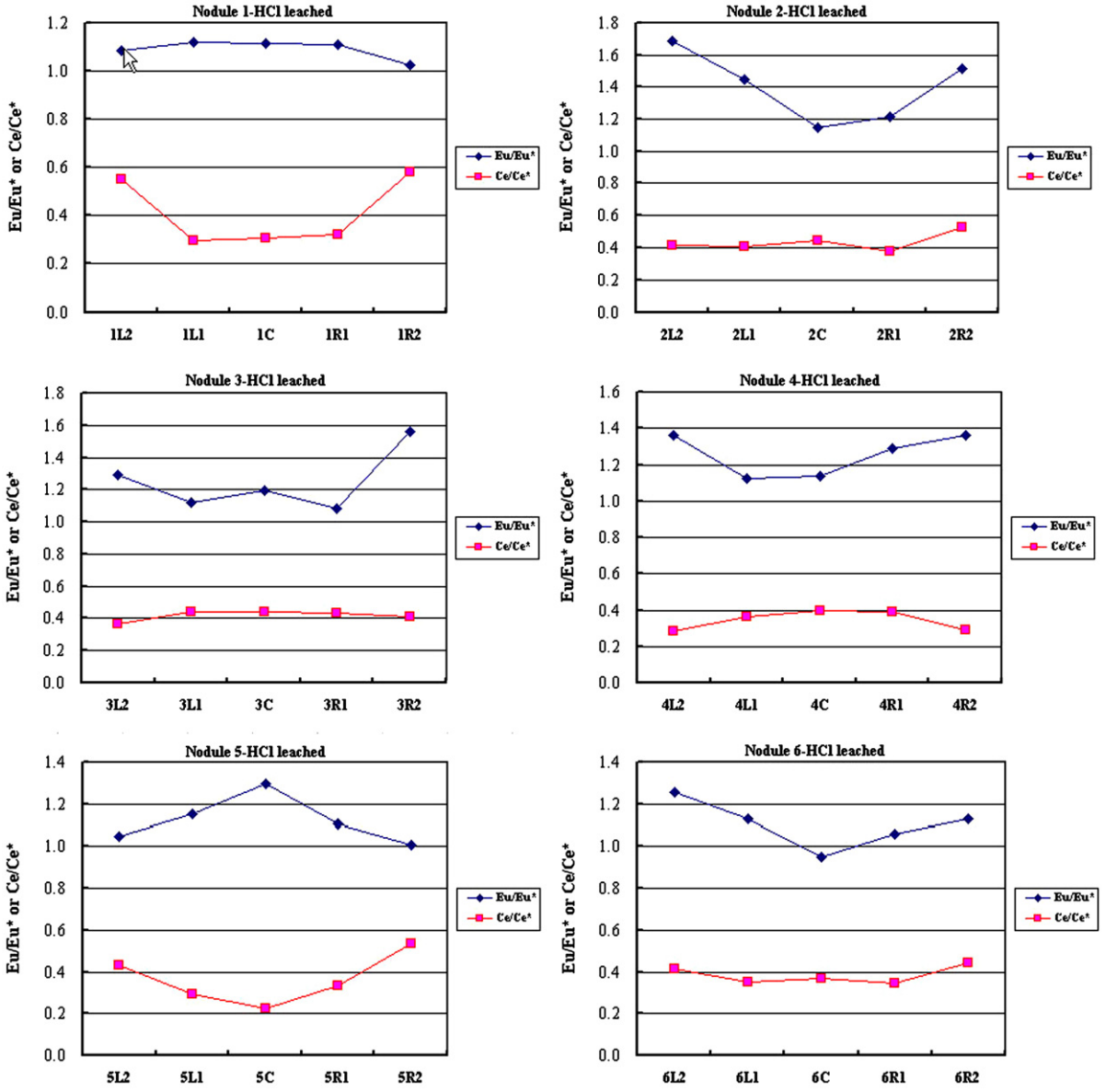

Fig. 8. Eu anomaly and Ce anomaly variation of the studied phosphate nodule traverse (HCl-leached) from the core to rim.

et al., 1985). Eu anomalies have been reported in various types of igneous and sedimentary rocks (Henderson, 1984). However, reduction of Eu does not seem to occur within the ocean basins except in submarine hydrothermal systems and during some extreme marine diagenesis in certain organic-rich, sulfate reducing environments (Michard et al., 1983; MacRae et al., 1992).

Positive Eu anomalies have been reported for some phosphorite occurrences and phosphate nodules hosting in organic-rich shales (Ogihara, 1999; Kidder et al., 2003). Our results for the HCl-leached phosphate nodules in the Early Cambrian organic-rich black shales also show positive Eu anomalies to variable extent, with higher Eu/Eu* values for the rims in most of the studied nodules. Commonly, positive Eu anomalies are interpreted as a result of extremely reducing conditions (Ogihara, 1999; Kidder et al., 2003). In such a reducing system, decay of organic matter would quickly use up the minimal available oxygen, and this might favor reduction of Eu^{3+} to Eu^{2+}, and then the Eu^{2+} could move into the phosphate nodules (Kidder et al., 2003). This explanation is consistent with the higher Eu/Eu* values in the phosphate nodule rims in our studied samples.

Table 4
Analytical results of selected trace element concentrations for the HAc-leached fractions of the phosphate nodules

ppm	1C	1L1	1L2	1R1	1R2	2C	2L1	2L2	2R1	2R2	3C	3L1	3L2	3R1	3R2
Mn	119	58.8	40.3	83.0	42.0	46.2	49.6	32.8	40.7	44.7	53.3	59.9	142.5	68.5	113.3
V	0.6	0.3	2.8	0.8	4.4	0.3	0.6	2.0	0.2	1.0	0.4	0.3	6.0	1.0	7.9
Cr	3.1	1.1	2.6	1.0	3.4	0.7	0.9	2.6	0.6	2.4	1.3	1.1	3.5	1.3	3.3
Mo	0.03	0.02	0.1	0.05	0.1	0.01	0.02	0.02	0.01	0.04	0.01	0.01	0.03	0.03	0.04
Ni	5.1	2.8	70.0	10.1	53.0	1.9	54.2	12.2	6.2	17.2	0.7	1.3	5.3	12.4	21.2
U	0.04	0.02	0.03	0.03	0.02	0.01	0.04	0.01	0.003	0.01	0.02	0.01	0.02	0.02	0.02
Sc	0.1	0.1	0.1	0.1	0.05	0.03	0.03	0.03	0.03	0.02	0.02	0.01	0.02	0.02	0.01
Ti	0.2	0.2	0.4	0.2	0.2	0.3	0.2	0.2	0.2	0.2	0.2	0.1	0.2	0.2	0.1
Co	2.3	1.6	3.3	2.4	2.7	1.2	0.8	2.2	1.2	1.8	0.6	0.5	1.9	0.9	1.4
Cu	0.4	0.2	0.3	0.3	0.2	0.1	0.1	0.1	0.1	0.2	0.1	0.1	0.1	0.1	0.2
Zn	3.0	4.3	3.9	4.3	4.7	5.2	3.2	2.6	3.2	4.2	2.8	1.8	2.4	1.9	4.4
Ga	0.3	0.4	0.4	0.3	0.3	0.3	0.2	0.2	0.3	0.2	0.2	0.2	0.1	0.1	0.1
Rb	0.9	1.1	1.8	1.2	1.9	0.7	0.7	1.8	1.2	1.5	0.7	0.9	1.4	0.8	1.6
Sr	694	533	407	477	326	741	501	401	602	406	591	576	495	489	446
Ba	249	287	278	329	225	314	195	428	396	398	259	245	212	211	202
Pb	1.3	0.3	0.7	1.7	1.3	0.5	8.7	0.4	0.3	5.8	0.4	0.4	5.0	0.5	8.8
Th	0.003	0.001	0.002	0.001	0.000	0.000	0.001	0.001	0.000	0.002	0.001	0.000	0.001	0.002	0.000
Rb/Sr	0.001	0.002	0.004	0.003	0.006	0.001	0.001	0.004	0.002	0.004	0.001	0.002	0.003	0.002	0.004
U/Th	11.7	41.6	11.1	46.1	66.6	24.2	54.2	9.5	9.5	5.9	16.5	30.8	15.6	9.9	37.6
Co/Ni	0.46	0.58	0.05	0.24	0.05	0.61	0.01	0.18	0.19	0.10	0.95	0.43	0.36	0.07	0.07
V/Ni	0.12	0.12	0.04	0.08	0.08	0.13	0.01	0.16	0.03	0.06	0.55	0.28	1.12	0.08	0.37

(continued on next page)

Table 4 (*continued*)

ppm	4C	4L1	4L2	4R1	4R2	5C	5L1	5L2	5R1	5R2	6C	6L1	6L2	6R1	6R2
Mn	65.6	71.4	25.2	38.1	29.8	21.8	35.7	20.9	43.9	37.5	29.6	33.5	29.7	47.7	22.8
V	0.2	0.8	1.4	0.3	2.1	0.1	0.6	0.9	0.8	2.1	0.4	0.4	2.3	1.4	2.7
Cr	0.9	1.9	3.5	1.7	3.1	1.7	4.7	5.3	3.3	4.2	3.1	3.4	4.9	3.0	4.6
Mo	0.01	0.02	0.03	0.01	0.03	0.01	0.02	0.03	0.01	0.02	0.01	0.01	0.04	0.04	0.1
Ni	2.5	2.0	6.2	1.4	2.5	2.4	2.3	5.0	1.1	3.0	2.3	3.6	11.2	49.8	25.7
U	0.02	0.02	0.03	0.02	0.1	0.01	0.01	0.01	0.01	0.02	0.05	0.02	0.03	0.02	0.04
Sc	0.02	0.01	0.01	0.01	0.01	0.01	0.01	0.02	0.01	0.02	0.02	0.02	0.01	0.01	0.02
Ti	0.1	0.1	0.1	0.1	0.1	0.1	0.1	0.1	0.1	0.1	0.2	0.1	0.1	0.5	0.1
Co	1.5	0.8	1.3	0.9	1.5	3.6	1.2	1.4	1.1	1.3	6.6	2.0	2.0	2.8	2.4
Cu	0.1	0.1	0.2	0.1	0.1	0.1	0.2	0.3	0.3	0.1	0.1	0.2	0.1	0.2	0.1
Zn	2.3	2.1	2.7	1.8	2.7	2.0	1.5	2.4	2.8	4.6	2.0	3.8	2.4	2.6	3.1
Ga	0.2	0.2	0.1	0.2	0.1	0.2	0.1	0.1	0.1	0.1	0.1	0.1	0.1	0.1	0.1
Rb	0.9	1.1	1.6	0.9	1.7	0.6	1.2	1.6	1.1	1.6	0.9	1.3	2.3	1.2	2.8
Sr	1085	796	352	829	381	569	482	524	514	513	661	523	369	657	282
Ba	303	331	334	316	340	274	214	334	279	270	277	490	317	424	300
Pb	1.3	0.7	1.7	0.5	1.2	1.9	2.8	0.5	1.1	0.8	0.3	1.3	1.0	0.8	0.9
Th	0.0005	0.001	0.001	0.001	0.001	0.003	0.001	0.0005	0.001	0.001	0.003	0.001	0.001	0.005	0.001
Rb/Sr	0.001	0.001	0.005	0.001	0.005	0.001	0.002	0.003	0.002	0.003	0.001	0.003	0.006	0.002	0.010
U/Th	34.2	19.4	40.7	12.8	59.2	4.2	8.8	24.8	12.0	36.3	17.5	13.2	30.1	4.3	41.1
Co/Ni	0.61	0.39	0.22	0.61	0.59	1.51	0.54	0.29	1.03	0.44	2.87	0.56	0.18	0.06	0.09
V/Ni	0.08	0.40	0.23	0.18	0.82	0.05	0.26	0.18	0.78	0.72	0.16	0.12	0.21	0.03	0.10

Table 5
Analytical results of selected trace element concentrations for the HCl-leached fractions of the phosphate nodules

ppm	1C	1L1	1L2	1R1	1R2	2C	2L1	2L2	2R1	2R2	3C	3L1	3L2	3R1	3R2
Mn	33.1	28.8	20.6	34.7	18.4	43.6	42.2	17.8	25.9	24.0	26.4	27.2	37.0	30.0	29.1
V	45.2	45.0	76.5	45.2	80.2	42.8	37.7	53.1	32.0	50.0	37.4	38.7	91.5	40.1	116
Cr	25.2	24.8	40.6	24.1	38.1	19.4	16.6	29.0	15.4	27.9	17.0	19.6	35.7	18.4	39.7
Mo	0.26	0.34	1.57	0.46	0.69	0.11	0.20	0.20	0.09	0.25	0.08	0.19	0.20	0.46	0.24
Ni	1.00	1.21	59.2	2.37	44.6	1.06	2.11	3.48	2.61	11.3	0.46	1.20	2.63	10.6	53.8
U	1.51	1.50	0.71	1.07	0.5	0.8	0.6	0.3	0.5	0.37	1.17	0.87	0.70	0.78	0.46
Sc	13.6	12.7	12.9	11.5	12.5	4.9	5.2	6.7	5.2	6.68	5.30	9.53	10.7	8.55	9.05
Ti	41.1	50.1	59.1	43.3	62.1	41.0	62.4	71.2	38.4	56.4	43.7	46.4	60.0	42.3	62.8
Co	0.26	0.29	0.47	0.37	0.38	0.24	0.25	0.36	0.20	0.33	0.15	0.18	0.26	0.23	0.31
Cu	0.78	1.82	3.98	1.61	2.18	0.70	0.45	1.41	0.58	1.26	1.13	1.45	3.55	1.28	2.08
Zn	40.3	32.7	30.3	38.2	28.1	50.0	39.0	50.1	34.8	44.5	89.2	29.4	30.9	26.3	21.9
Ga	0.90	1.00	1.62	0.90	1.86	0.67	0.46	1.03	0.50	0.90	0.73	0.73	1.06	0.70	1.25
Rb	3.41	3.59	5.69	3.33	5.80	1.79	2.15	4.48	1.78	4.61	2.43	2.60	4.75	2.67	5.49
Sr	2792	1975	1355	1614	1120	2663	2321	1248	1661	1261	2451	2552	1426	2373	1484
Ba	2071	1562	1141	1686	817	2952	2412	3397	1951	2873	6144	2107	1603	1875	1146
Pb	0.69	0.72	0.93	0.44	0.81	0.12	0.26	0.34	0.23	0.41	0.22	1.79	1.03	0.57	0.69
Th	0.26	0.23	0.23	0.21	0.23	0.07	0.13	0.18	0.12	0.24	0.14	0.20	0.39	0.20	0.33
Rb/Sr	0.001	0.002	0.004	0.002	0.005	0.001	0.001	0.004	0.001	0.004	0.001	0.001	0.003	0.001	0.004
U/Th	5.83	6.40	3.14	5.16	2.09	11.7	4.95	1.57	4.01	1.56	8.12	4.43	1.80	3.98	1.39
Co/Ni	0.26	0.24	0.01	0.16	0.01	0.23	0.12	0.10	0.08	0.03	0.33	0.15	0.10	0.02	0.01
V/Ni	45.2	37.07	1.29	19.1	1.80	40.3	17.9	15.3	12.3	4.45	81.9	32.3	34.8	3.78	2.16

(continued on next page)

Table 5 (*continued*)

ppm	4C	4L1	4L2	4R1	4R2	5C	5L1	5L2	5R1	5R2	6C	6L1	6L2	6R1	6R2
Mn	37.6	29.0	14.4	24.3	17.0	27.7	21.2	14.9	27.7	21.2	26.6	18.3	14.9	24.8	15.4
V	24.9	38.9	63.9	28.5	61.8	30.9	36.6	53.3	41.3	54.5	24.1	26.5	47.9	25.3	44.9
Cr	16.9	20.5	36.4	18.1	35.3	20.1	25.7	36.8	25.4	35.6	20.5	18.1	33.7	19.1	31.8
Mo	0.11	0.25	0.20	0.10	0.21	0.10	0.12	0.25	0.11	0.19	0.13	0.09	0.29	2.50	0.54
Ni	1.40	1.94	6.26	1.17	2.76	0.76	1.34	2.35	1.31	2.40	1.08	1.09	2.49	36.8	26.7
U	1.40	0.75	0.74	0.89	1.28	0.99	0.28	0.45	0.27	0.52	1.42	0.66	0.44	0.54	0.60
Sc	8.40	9.36	10.08	8.00	9.79	8.63	9.42	14.9	13.3	15.3	11.9	8.28	10.7	8.64	11.7
Ti	50.0	53.1	79.8	40.8	80.4	36.5	51.2	70.2	47.8	63.3	46.5	49.0	73.4	47.2	75.5
Co	0.21	0.18	0.29	0.19	0.33	0.34	0.24	0.29	0.29	0.31	0.92	0.30	0.47	0.54	0.70
Cu	2.18	1.53	3.89	1.17	4.10	0.68	0.91	3.85	1.17	1.65	1.32	1.30	1.98	2.53	2.23
Zn	48.0	59.5	58.5	42.6	43.6	19.9	32.0	20.0	19.0	16.9	39.7	52.9	24.8	56.8	57.0
Ga	0.80	0.67	1.07	0.63	1.29	0.59	0.62	1.15	0.87	2.10	0.70	0.92	1.31	0.87	1.29
Rb	2.43	2.70	4.93	1.67	5.37	1.80	2.60	4.62	2.60	4.97	2.77	3.48	6.46	2.87	6.48
Sr	3264	2435	1293	2758	1268	1771	1813	2149	2092	2240	2097	1443	1003	2353	873
Ba	3644	4818	4761	3651	3437	1457	2394	1033	1219	1091	2668	3494	1669	3648	3605
Pb	0.55	0.59	1.66	0.33	1.91	0.57	0.74	1.26	0.53	0.91	0.87	1.74	1.10	0.63	1.25
Th	0.37	0.25	0.36	0.26	0.23	0.23	0.21	0.36	0.22	0.47	0.22	0.34	0.30	0.31	0.44
Rb/Sr	0.001	0.001	0.004	0.001	0.004	0.001	0.001	0.002	0.001	0.002	0.001	0.002	0.006	0.001	0.007
U/Th	3.78	2.96	2.06	3.42	5.63	4.24	1.33	1.26	1.23	1.10	6.39	1.92	1.46	1.75	1.35
Co/Ni	0.15	0.09	0.05	0.16	0.12	0.45	0.18	0.12	0.22	0.13	0.85	0.27	0.19	0.01	0.03
V/Ni	17.8	20.0	10.2	24.4	22.4	40.5	27.4	22.6	31.4	22.7	22.2	24.3	19.2	0.69	1.68

Alternatively, a hydrothermal fluid component can also cause significant positive Eu anomalies (Michard et al., 1983, Stalder and Rozendaal, 2004). In our case, we believed that the positive Eu anomalies were more likely caused by redox conditions, because Eu^{3+} can be readily reduced into Eu^{2+} in reducing conditions and the Eu^{2+} can replace Ca^{2+} easily in the phosphate minerals. If this were the case, the degree of the Eu anomaly would indicate that the sedimentary environment had changed from suboxic/dysoxic to anoxic conditions during the nodule formation. It needs to point out that we can not totally rule out the contribution of submarine hydrothermal fluid to the phosphate nodule formation, since a number of studies have suggested a submarine hydrothermal origin for the Ni–Mo sulfide bed within the same host black shale sequence in south China (Steiner et al., 2001; Jiang et al., 2006, in press). However, clear evidence pointing to this hydrothermal origin is still lacking, and more work need to be done in this regard.

5.3. Ce anomaly

Ce anomalies have been found exclusively in ocean basins, with seawater being typically depleted in Ce with respect to its REE neighbours La and Pr (Elderfield and Greaves, 1982; De Baar et al., 1985). It is suggested that the extent of Ce anomaly in seawater is mainly controlled by the redox conditions and has been used as a tracer to distinguish between anoxic and oxic water bodies in the geological past (Wright et al., 1987; German and Elderfield, 1990). In addition, factors such as microbial activity that catalyses the oxidation of Ce^{3+}, the pH, water depth, and age of the seawater body may have also played a role in affecting the Ce anomaly (German and Elderfield, 1990; Moffett, 1990).

Negative Ce anomalies are observed for both the HCl-leached and HAc-leached fractions of the phosphate nodules (Figs. 5, 6). It is possibly a result of the source being ambient seawater with a pronounced Ce depletion (Morad and Felitsyn, 2001). Negative Ce anomalies are common in Cenozoic reworked phosphates and have been interpreted as reflecting oxidation by seawater (McArthur and Walsh, 1984). Shields and Stille (2001) suggested that the negative Ce anomalies may reflect a redox-stratified ocean during the Early Cambrian time in south China. They proposed that ocean stratification is actually a prerequisite for the development of phosphogenic systems (Shields and Stille, 2001). In this study, we found that all of the phosphate nodule cores show pronounced negative Ce anomaly with $Ce/Ce^* < 0.4$, whereas some of the phosphate nodule rims display less Ce anomaly with $Ce/Ce^* > 0.4$ (Fig. 8). It is likely that the early stage of the phosphate nodule growth may occur above the redox boundary, which will be more likely to retain the seawater-like negative Ce anomaly. The late stage of the phosphate nodule formation may end up below the redox boundary, and tend to undergo considerably more REE remobilization due to higher REE availability and reducing conditions during REE scavenging (Shields and Stille, 2001).

5.4. Redox-sensitive trace element composition

Previous studies have demonstrated that some redox-sensitive metals, such as Mo, V, Ni, Cr, U, and Mn, in marine sediments can yield powerful information linked to local or global paleo-oceanographic variability (Anderson et al., 1989; Yarincik et al., 2000; Yang et al., 2004). Anoxic sediments are typically enriched in Mo, V, Ni, Cr and U (Lewan and Maynard, 1982; Anderson et al., 1989; Wignall, 1994), while oxidized sediments are likely enriched in Mn, leading in places to Fe–Mn oxides and crusts.

In this study, almost all of the HCl-leached fractions of the phosphate nodules show an increase in contents of Mo, V, Ni and Cr from the core to rim (Fig. 9). However, the concentrations of U and Mn decrease from the core to rim (Fig. 9). It is likely that the increase of the redox-sensitive metals record the changing redox conditions during nodule growth. The decreases in Mn along with nodule growth indicate a progressively more reducing diagenesis, because reducing process produces soluble Mn^{2+}, which diffuses away from the site of reduction (Morford et al., 2001). The V, Cr, Ni and Mo concentrations are thought to coincide with reducing conditions (Lewan and Maynard, 1982; Anderson et al., 1989; Wignall, 1994). Commonly, these elements are associated with organic matter, and during the progress of diagenesis, decay of the organic matter may release these elements and caused the increase of these elements in the phosphate nodule rims in our study. The high Ba contents in the phosphate nodules may also relate to the decomposition of organic matter that release bio-barite and cause Ba mobile during anoxic diagenesis. Torres et al. (1996) have documented a diagenetic mechanism by which biogenic barium is remobilized in the sulfate reducing zone, moves up and reprecipitates as disseminated barite grains or veinlets.

5.5. Origin of the phosphate nodules and palaeoenvironment

Marine phosphate deposits occur along many of the continental margins in the world as nodules, irregular

masses, sands, pellets, and oolites (Burnett, 1977). The origin of these phosphate deposits has long been debated. Some early researchers invoked direct inorganic precipitation of marine phosphorite from seawater (e.g., Kazakov, 1937). Marine phosphate may precipitate from pore waters of anoxic sediments, and Burnett (1977) suggested that the phosphate content within the pore waters is generally higher than the overlying bottom waters by as much as several orders of magnitude. Experimental data have shown that Mg^{2+} ions inhibit the precipitation of apatite (Martens and Harriss, 1970), but diagenetic reactions could significantly deplete anoxic pore waters of Mg^{2+} that raise the Ca/Mg ratios of the pore waters to the point where apatite may precipitate (Burnett, 1977).

The supply of dissolved phosphate ions in pore waters is a prerequisite for phosphate precipitation. Stumm and Leckie (1970) invoked two mechanisms to supply phosphate ions to anoxic pore waters. One is from the decomposition of phosphorus-containing organic materials, and another is from the reduction of hydrous ferric oxides that bind phosphate to their surfaces under reducing conditions. REE concentrations in phosphate nodules are up to 50–100 times higher than shale-normalized values, which are several orders of magnitude greater than bulk

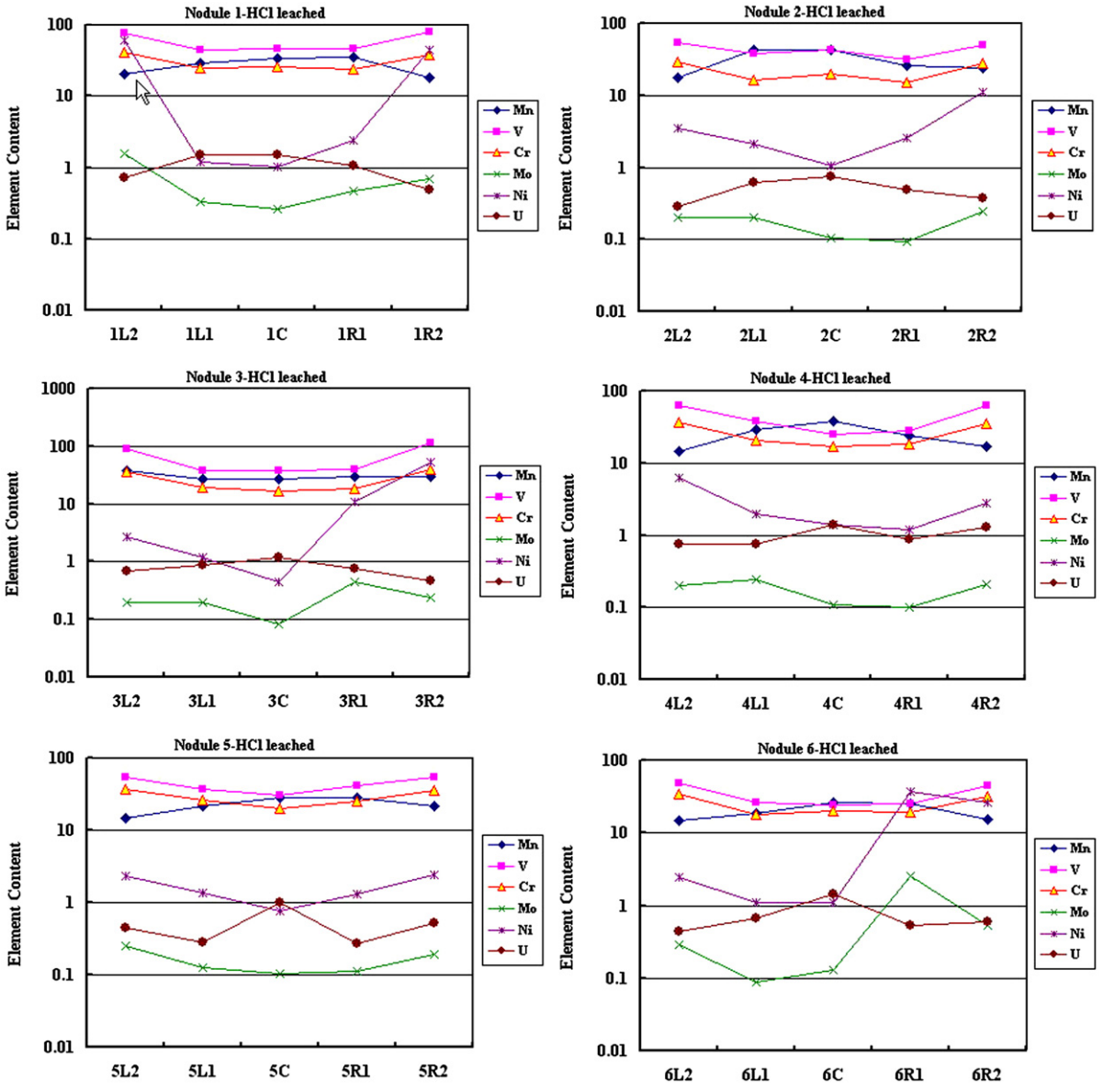

Fig. 9. Redox-sensitive trace element variation of the studied phosphate nodule traverse (HCl-leached) from the core to rim.

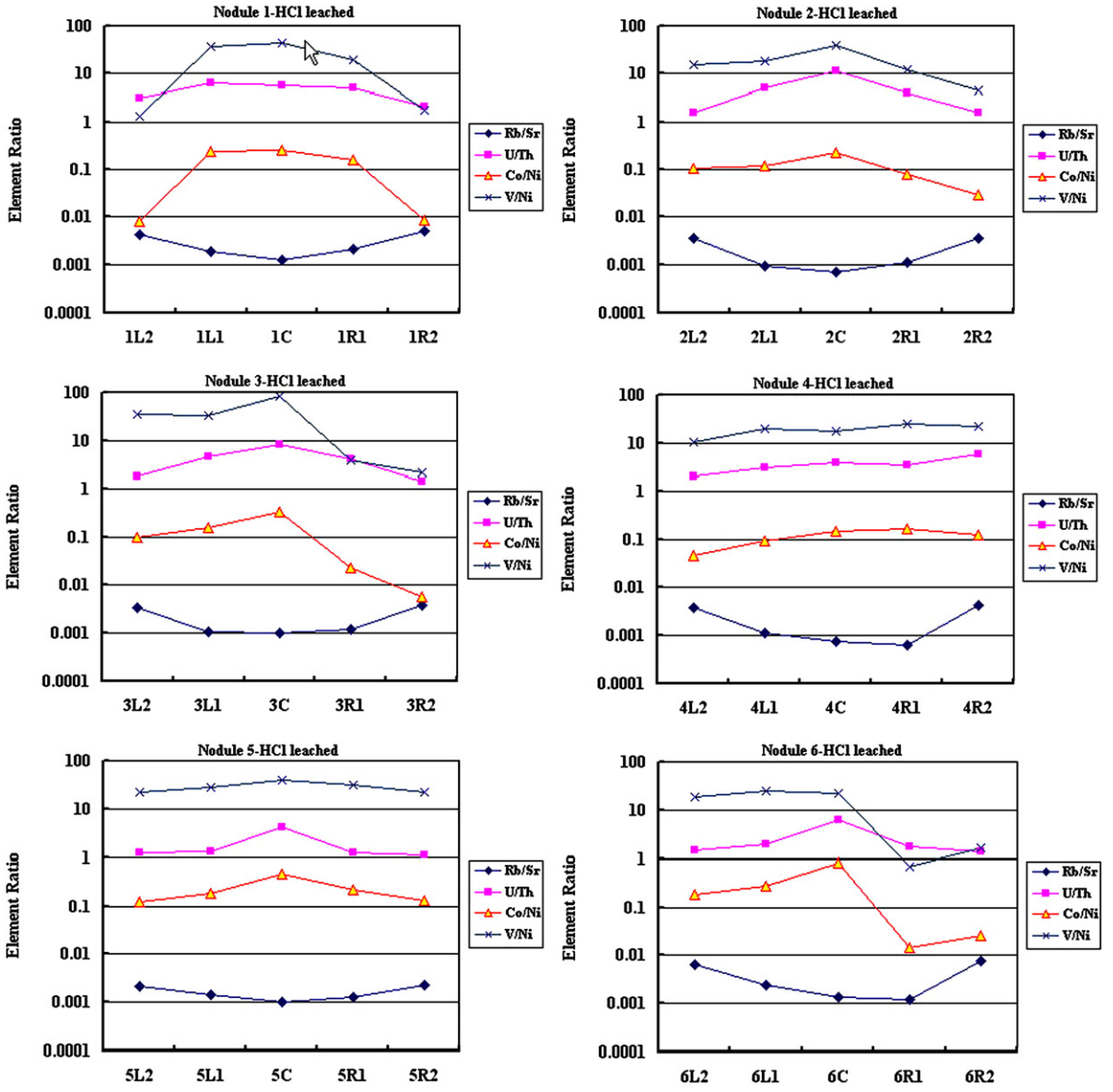

Fig. 10. Variation in trace element ratios of the studied phosphate nodule traverse (HCl-leached) from the core to rim.

REE content in seawater (Elderfield and Greaves, 1982). Therefore, Felitsyn and Morad (2002) believed that direct extraction of REE from marine pore waters can be precluded as the most important mechanism to explain the REE enrichment in authigenic phosphate, and they suggested that organic matter might have been the most important source of REE in phosphate nodules. In addition, Stalder and Rozendaal (2004) suggested a source of hydrothermal fluid for phosphate and REE, which may be also a likely factor in our studied case.

In Fig. 11, we propose a genetic model for the formation of abundant phosphate nodules in the Lower Cambrian black shale in south China. In this model, seawater can be divided into three layers based on redox conditions, i.e., the upper oxic layer with dissolved oxygen from atmosphere; the middle dysoxic layer as a result of continuously replenish of oxic benthic flux, and the bottom anoxic layer. In this system, major phosphorite deposits may precipitate on shelf or slop in suboxic/anoxic conditions, in connection with upwelling of nutrient rich water (Trappe, 1998), while phosphate nodules form after the strong upwelling stage in an organic-rich basin of deeper seawater. Near the sediment–water interface of seafloor, where most of the

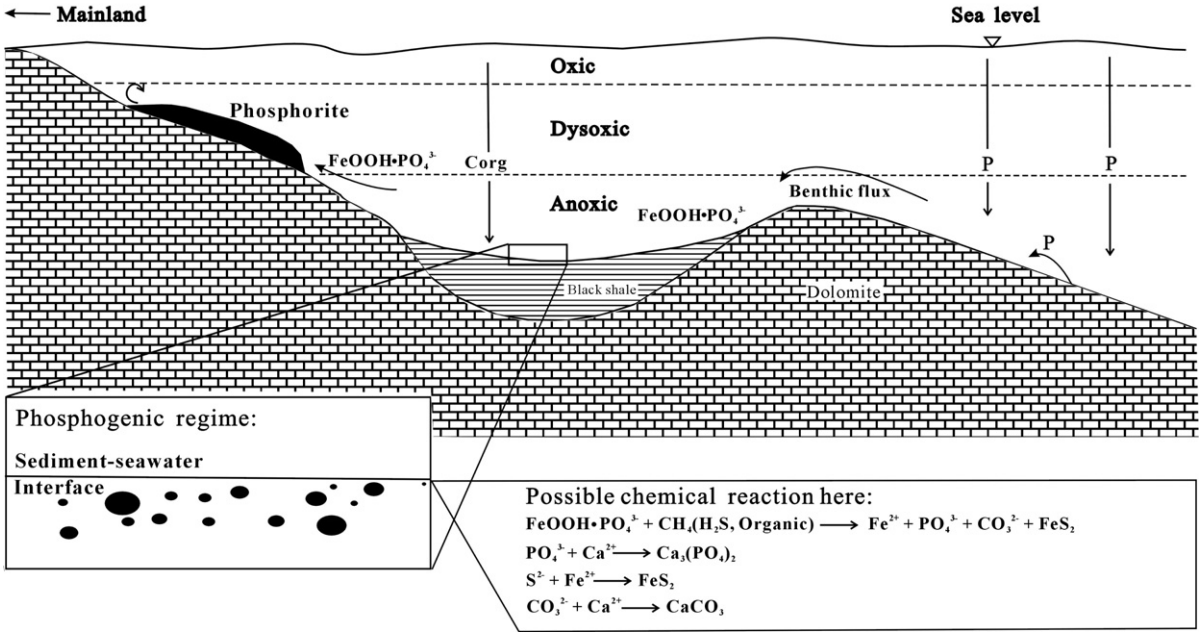

Fig. 11. Model for phosphate nodule and phosphorite formation in the Lower Cambrian black shale strata in south China.

freshly settled organic material is oxidized, phosphate is released to the sediment pore water from which it can escape to the overlying water (Martens et al., 1978). Alternatively, phosphate can be adsorbed to iron oxides and move with benthic flux (Krom and Berner, 1980; Slomp et al., 1998), which bring large amount of REEs and trace elements like Mo, V, and Ni. When the benthic flux pass an organic-rich basin, parts of the Fe–Mn oxyhydroxides in flux will be reduced and enter pore water together with P and REEs. PO_4^{3-} will combine with Ca^{2+} to form nodular phosphate, and lot of REEs and trace elements are incorporated into nodules. Fe^{2+} would go down and deposit as FeS_2 (Froelich et al., 1988) when encountering H_2S, which may either come from hydrothermal or from reduction of marine sulfates.

6. Conclusions

a) Phosphate nodules from the Lower Cambrian black shales in the Mufu Mountain section in south China are symmetrical in geochemistry with an increase of REE and a number of redox-sensitive trace elements such as V, Cr, Ni, and Mo from the core to rim. The variations of trace element concentrations can be interpreted as that phosphate formed from seawater and diagenetic pore fluid during diagenetic processes.
b) The phosphate nodule cores show seawater-like shale-normalized REE patterns, which may represent the characteristics of the Early Cambrian seawater. In contrast, the phosphate nodule rims display MREE-rich and HREE-depleted patterns, possibly resulting from significant diagenetic effect, with REE-rich pore fluid deriving after organic decay during later diagenesis.
c) Phosphorus in phosphate nodules was likely originated from seawater, coagulated by ferric oxyhydroxides adsorption or released by degradation of organic matter, enriched in seawater-sediments interface, and deposited in an organic-rich ocean basin.

Acknowledgements

This study is financially supported by a grant from China National Science Foundation (41221301) and a Key Project of the Ministry of Education of China (306007). The authors would like to thank all members in the Sino-German Cooperative Program on “From Snowball Earth to the Cambrian Bioradiation: A Multidisciplinary Analysis of Yangtze Platform, China” for their thoughtful discussion and encouragement. Drs. Lynn Walter, David Kidder, Graham Shields, Qingjun Guo, and Hartwig Frimmel provided very useful reviews and suggestions that improved this paper significantly.

References

Anderson, R.F., Fleisher, M.Q., LeHuray, A.P., 1989. Concentration, oxidation state, and particulate flux of uranium in the Black Sea. Geochimica et Cosmochimica Acta 53, 2215–2224.

Bertrand-Sarfati, J., Flicoteaux, R., Moussine-Pouchkine, A., Ahmed, A.A.K., 1997. Lower Cambrian apatitic stromatolites and phospharenites related to the glacio-eustatic cratonic rebound (Sahara, Algeria). Journal of Sedimentary Research 67, 957–974.

Birch, G.F., 1979. Phosphatic rocks on the western margin of South Africa. Journal of Sedimentary Petrology 49, 93–110.

Burnett, W.C., 1977. Geochemistry and origin of phosphorite deposits from off Peru and Chile. Geological Society of America Bulletin 88, 813–823.

Chen, Y., Jiang, S., Ling, H., Feng, H., Yang, J., Chen, J., 2003. Pb–Pb isotope dating of black shales from the Lower Cambrian Niutitang formation, Guizhou Province, South China. Progress in Natural Science 13, 771–776.

De Baar, H.J.W., Bacon, M.P., Brewer, P.G., 1985. Rare Earth Elements in pacific and Atlantic Oceans. Geochimica et Cosmochimica Acta 49, 1943–1959.

Elderfield, H., Upstill-Goddard, R., Sholkovitz, E.R., 1990. The rare earth elements in rivers, estuaries, and coastal seas and their significance to the composition of ocean waters. Geochimica et Cosmochimica Acta 54, 971–991.

Elderfield, H., Greaves, M.J., 1982. The rare earth elements in seawater. Nature 296, 214–219.

Elderfield, H., Pagett, R., 1986. Rare Earth elements in Ichthyoliths: variations with redox conditions and depositional environment. In: Riley, J.P. (Ed.), Sciences of the Total Environment, vol. 49, pp. 175–197.

Elderfield, H., Sholkovitz, E.R., 1987. Rare earth elements in the pore waters of reducing nearshore sediments. Earth and Planetary Science Letters 82, 280–288.

Felitsyn, S., Morad, S., 2002. REE patterns in latest Neoproterozoic-early Cambrian phosphate concretions and associated organic matter. Chemical Geology 187, 257–265.

Froelich, P.N., Arthur, M.A., Burnett, W.C., Deakin, M., Hensley, V., Jahnke, R., Kaul, L., Kim, K.-H., Roe, K., Soutar, A., Vathakanon, C., 1988. Early diagenesis of organic matter in Peru continental margin sediments: phosphorite precipitation. Marine Geology 80, 309–343.

German, C.R., Elderfield, H., 1990. Application of the Ce anomaly as a paleoredox indicator: the ground rules. Paleooceanography 5, 823–833.

Grandjean-Lecuyer, P., Feist, R., Albarede, F., 1993. Rare earth elements in old biogenic apatite. Geochimica et Cosmochimica Acta 57, 2507–2514.

Henderson, P., 1984. Rare Earth Element Geochemistry. Elservier, Amsterdam. 510pp.

Ilyin, A.V., 1998. Rare earth geochemistry of "old" phosphorites and probability of syngenetic precipitation and accumulation of phosphate. Chemical Geology 144, 243–256.

Jiang, S.Y., Chen, Y.Q., Ling, H.F., Yang, J.H., Feng, H.Z., Ni, P., 2006. Trace-and rare-earth element geochemistry and Pb–Pb dating of black shales and intercalated Ni–Mo–PGE–Au sulfide ores in Lower Cambrian strata, Yangtze Platform, South China. Mineralium Deposita 126 (66), 1–18.

Jiang, S.Y., Yang, J.H., Ling, H.F., Chen, Y.Q., Feng, H.Z., Zhao, K.D., Ni, P., in press. Extreme enrichment of polymetallic Ni-Mo-PGE-Au in Lower Cambrian black shales of South China: an Os isotope and PGE geochemical investigation. Palaeogeography, Palaeoclimatology, Palaeoecology. doi:10.1016/j.palaeo.2007.03.024.

Kazakov, A.V., 1937. The phosphorite facies and the genesis of phosphorites. Geological investigations of agricultural ores. USSR Science Institution of Fertilizers and Insectofungicides 142, 93–113.

Kennedy, W.J., Garrison, R.E., 1975. Morphology and genesis of nodular chalks and hardgrounds in the Upper Cretaceous of southern England. Sedimentology 22, 311–386.

Kidder, D.L., Eddy-Dilek, C.A., 1994. Rare-earth element variation in phosphate nodules from midcontinent Pennsylvanian cyclothems. Journal of Sedimentary Research A 64, 584–592.

Kidder, D., Krishnaswamy, R., Mapes, R.H., 2003. Elemental mobility in phosphatic shales during concretion growth and implication for provenance analysis. Chemical Geology 198, 335–353.

Krom, M., Berner, R., 1980. Adsorption of phosphate in anoxidized-marine sediments. Limnology and Oceanography 25, 797–806.

Lewan, M.D., Maynard, J.B., 1982. Factors controlling enrichment of vanadium and nickel in the bitumen of organic sedimentary rocks. Geochimica et Cosmochimica Acta 46, 2547–2560.

MacRae, N.D., Nesbitt, H.W., Kronberg, B.I., 1992. Development of a positive Eu anomaly during diagenesis. Earth and Planetary Science Letters 109, 585–591.

Martens, C.S., Harriss, R.C., 1970. Inhibition of apatite precipitation in the marine environment by magnesium ions. Geochimica et Cosmochimica Acta 34, 621–625.

Martens, C., Berner, R., Rosenfeld, J., 1978. Interstitial water chemistry of anoxidized Long Island Sound sediments: 2. Nutrient regenerationand phosphate removal. Limnology and Oceanography 23, 605–617.

McArthur, J.M., Walsh, J.N., 1984. Rare Earth of geochemistry of phosphorite. Chemical Geology 47, 191–220.

Marshall-Neil, G., Ruffell, A., 2004. Authigenic phosphate nodules (Late Cretaceous, northern Ireland) as condensed succession microarchives. Cretaceous Research 25, 439–452.

Michard, A., Albarede, F., Michard, G., Minster, J.F., Charlou, J.L., 1983. Rare-Earth Elements and uranium in high-temperature solutions from East Pacific rise hydrothermal vent field (13°N). Nature 303, 795–797.

Morad, S., Felitsyn, S., 2001. Identification of primary Ce-anomaly signatures in fossil biogenic apatite: implication for the Cambrian oceanic anoxia and phophogenesis. Sedimentary Geology 143, 259–264.

Morford, J.L., Russell, A.D., Emerson, S., 2001. Trace metal evidence for changes in redox environment associated with the transition from terrigenous clay to diatomaceous sediment, Saanich Inlet, BC. Marine Geology, 174, 355–369.

Moffett, J.W., 1990. Microbially mediated cerium oxidation in seawater. Nature 345, 421–423.

O'Brien, G.W., Harris, J.R., Milnes, A.R., Veeh, H.H., 1981. Bacterial origin of east Australian continental margin phosphorites. Nature 294, 442–444.

Ogihara, S., 1999. Geochemical characteristics of phosphorite and carbonate nodules from the Miocene Funakawa Formation, western margin of the Yokote Basin, northeast Japan. Sedimentary Geology 125, 69–82.

Picard, S., Le'cuyer, C., Barrat, J.-A., Garcia, J.-P., Dromart, G., Sheppard, S.M.F., 2002. Rare earth element contents of Jurassic fish and reptile teeth and their potential relation to seawater composition (Anglo–Paris Basin, France and England). Chemical Geology 186, 1–16.

Rasmussen, B., Buick, R., Taylor, W.R., 1998. Removal of oceanic REE by authigenic precipitation of phosphatic minerals. Earth and Planetary Science Letters 164, 135–149.

Schuffert, J.D., Jahnke, R.A., Kastner, M., Leather, J., Sturz, A., Wing, M.R., 1994. Rates of formation of modern phosphorite off western Mexico. Geochimica et Cosmochimica Acta 58, 5001–5010.

Shields, G., Stille, P., 2001. Diagenetic constraints on the use of cerium anomalies as paleoseawater redox proxies: an isotope and REE study of Cambrian phosphorites. Chemical Geology 175, 29–48.

Sholkovitz, E.R., Piepgras, D.J., Jacobsen, S.B., 1989. The pore water chemistry of rare earth elements in Buzzards Bay sediments. Geochimica et Cosmochimica Acta 53, 2847–2856.

Slomp, C., Malschaert, J., Van Raaphorst, W., 1998. The role of adsorption in sediment–water exchange of phosphate in NorthSea continental margin sediments. Limnology and Oceanography 43, 835–846.

Stalder, M., Rozendaal, A., 2004. Apatite nodules as an indicator of depositional environment and ore genesis for the Mesoproterozoic Broken Hill-type Gamsberg Zn–Pb deposit, Namaqua Province, South Africa. Mineralium Deposita 39, 189–203.

Stanley Jr., J.K., Byrne, R.H., 1990. The influence of solution chemistry on REE uptake by *Ulva lactuca* L. in seawater. Geochimica et Cosmochimica Acta 54, 1587–1595.

Steiner, M., Wallis, E., Erdtmann, B.D., Zhao, Y., Yang, R., 2001. Submarine-hydrothermal exhalative ore layers in black shales from South China and associated fossils-insight into a lower Cambrian facies and bio-evolution. PALAEO 169, 165–191.

Stumm, W., Leckie, J.O., 1970. Phosphate exchange with sediments: its role in the productivity of surface water. In: Advances in water pollution research, 2, III26/1-26/16. New York, Pergamon Press.

Tlig, S., Sassi, A., Belayouni, H., Michel, D., 1987. Distribution de l'uranium de thorium du zirconium de hafnium de desterres rares (TR) dans les grains de phosphates sedimentaries. Chemical Geology 62, 209–221.

Torres, M.E., Brumsack, H.J., Bohrmann, G., Emeis, K.C., 1996. Barite fronts in continental marine sediments: a new look at barium remobilisation in the zone of sulfate reduction and formation of heavy barites in diagenetic fronts. Chemical Geology 127, 125–139.

Trappe, J., 1998. Phanerozoic phosphorite depositional systems. Lecture Notes in Earth Sciences, vol. 76. Springer, Berlin. 316pp.

Veeh, H.H., Burnett, W.C., Soutar, A., 1973. Contemporary phosphorites on the continental margin of Peru. Science 181, 844–845.

Walsh, J.J., 1981. A carbon budget for overfishing off Peru. Nature 290, 300–304.

Wignall, P.B., 1994. Black shales. Claredon Press, Oxford. 127pp.

Wright, J., Schrader, H., Holser, W.T., 1987. Paleoredox variations in ancient oceans recorded by rare earth elements in fossil apatite. Geochimica et Cosmochimica Acta 51, 631–644.

Yang, J.H., Jiang, S.Y., Ling, H.F., Feng, H.Z., Chen, Y.Q., Chen, J.F., 2004. Paleoceangraphic significance of redox-sensitive metals of black shales in the basal Lower Cambrian Niutitang Formation in Guizhou Province, South China. Progress in Natural Science 14, 152–157.

Yarincik, K.M., Murray, R.W., Lyons, T.W., Peterson, L.C., Haug, G.H., 2000. Oxygenation history of bottom waters in the Cariaco Basin, Venezuela, over the past 57,8000 years: results from redox-sensitive metals (Mo, V, Mn, and Fe). Paleoceanography 15 (6), 593–601.

Zhu, M.Y., Zhang, J.M., Steiner, M., Yang, A., Li, G., Erdtmann, B.D., 2003. Sinian-Cambrian stratigraphic framework for shallow-to deep-water environments of the Yangtze Platform: an integraed approach. Progress in Natural Science 13, 951–960.